Enhancing Urban Pluvial Flood Modelling through Graph Reconstruction of Incomplete Sewer Networks

Ruidong Li¹, Jiapei Liu¹, Ting Sun², Jian Shao³, Fuqiang Tian¹, and Guangheng Ni¹

¹State Key Laboratory of Hydro-science and Engineering, Department of Hydraulic Engineering, Tsinghua University, Beijing 100084, China

Correspondence: Ruidong Li (lyy0744@mail.tsinghua.edu.cn) and Ting Sun (ting.sun@ucl.ac.uk)

Abstract.

This work presents an efficient graph reconstruction-based approach for generating physical sewer models from incomplete information, addressing the challenge of representing sewer drainage effect in urban pluvial flood simulation. The approach utilizes graph-based topological analysis and hydraulic design constraints to derive gravitational flow directions and nodal invert elevations in decentralized sewer networks with multiple outfalls. By incorporating linearized programming formulation to solve reconstruction problems, this approach can achieve high computational efficiency, enabling application to city-scale sewer networks with thousands of nodes and links. Tested in Yinchuan, China, the approach integrates with a 1D/2D coupled hydrologic-hydrodynamic model and accurately reproduces maximum inundation depths ($R^2 = 0.95$) when the complete network layout and regulated facilities are available. Simplifications, such as adopting road-based layouts and omitting regulation facilities, can degrade simulation performance for extreme rainfall events compared to calibrated equifinal methods. However, design rainfall analysis demonstrates that the physical reconstruction approach can reliably outperform equifinal methods, achieving reduced variation and higher accuracy in simulating inundation areas. However, proper configuration of regulated facilities and network connectivity remains crucial, particularly for simulating local inundation during extreme rainfall. Thus, it is recommended to integrate the proposed algorithm with targeted field investigations to further improve urban pluvial flood simulation performance in data-scarce regions.

1 Introduction

Global climate change and intensified human activities have significantly altered climatic conditions and surface environments, leading to an increase in the frequency and magnitude of urban pluvial floods, particularly where rainfall exceeds the design capacity of drainage systems (Rosenzweig et al., 2018). As representative drainage infrastructure, sewer networks can effectively mitigate pluvial flood risks by transporting rainwater to downstream sites such as river channels and detention ponds (Wang et al., 2022). However, its performance can be inherently insufficient and gradually deteriorate due to outdated design and poor maintenance (Tran et al., 2024), potentially resulting in system overflow and exacerbated surface floods during extreme rainfall

²Department of Risk and Disaster Reduction, University College London, London WC1E 6BT, UK

³Yinchuan Meteorological Bureau, Yinchuan 750002, China

(Schmitt and Scheid, 2020). Thus, accurately modeling the drainage effects of sewer networks is essential for urban pluvial flood simulation and risk attribution (Luan et al., 2024).

25

35

40

However, detailed sewer network information may not always be readily available and its implementation in hydraulic models requires laborious work with high uncertainty (Montalvo et al., 2024). As a result, various simplified approaches have been developed to approximate the effect of sewer drainage. These approaches typically introduce a term of sewer-induced mass loss during rainfall-runoff simulations within specific regions, such as roads and inlets (Li et al., 2020; Xing et al., 2021, 2019). However, such approaches fail to explicitly consider the relative difference in hydraulic heads between sewer networks and surface water, and thus are incapable of capturing critical processes such as overflow caused by system overload. To address these limitations, Montalvo et al. (2024) proposes a physics-based approach that designs a representative virtual sewer network using publicly available datasets and local design standards. This approach enables the development of a physical sewer hydraulic model with bidirectional interactions between surface and sewer flows, thereby offering a more comprehensive representation of sewer drainage processes. The virtual network design (VND) consists mainly of two steps:

- Layout Definition. This step determines the geometric connections and hydraulic directions between nodes in the sewer network. Typical algorithms include surface-elevation-driven delineation (Blumensaat et al., 2012; Duque et al., 2022), graph-theory-based modeling (Bakhshipour et al., 2019; Kim et al., 2021), and street-network-guided configuration (Chegini and Li, 2022; Reyes-Silva et al., 2023). Most existing work assumes the target system as a centralized layout with a single outfall (Hesarkazzazi et al., 2022), facilitating the application of tree-based solutions such as the minimum spanning tree (Reyes-Silva et al., 2023) and the Steiner minimal tree (Machine Hsie and Huang, 2019). However, this simplification ignores the rich topological structures of real-world decentralized networks with potential cycles and forests (Bakhshipour et al., 2019). Furthermore, most approaches assume that gravitational flow direction aligns with surface gradients—an assumption that may not hold in flat urban areas or in the presence of inaccurate elevation data (Hesarkazzazi et al., 2022; Dunton and Gardoni, 2024).
- Hydraulic Design. This step determines the sizes and slopes of pipes, as well as the necessary configuration of rainwater treatment facilities, with the objective of satisfying the design discharge requirement estimated by the Rational Method (Wang and Wang, 2018; Reyes-Silva et al., 2023). To achieve this, most approaches formulate the design task as an optimization problem and employ mathematical programming techniques such as linear programming (Swamee and Sharma, 2013), mixed-integer linear programming (Safavi and Geranmehr, 2017), nonlinear programming (Li and Matthew, 1990), and multi-objective programming (Bakhshipour et al., 2021). However, it requires significant computational efforts to obtain global optima in nonlinear or integer cases. Thus, approximate approaches such as piecewise linearization (Elimam et al., 1989), evolutionary algorithms (Wang et al., 2017; Bakhshipour et al., 2021), and topological-driven prediction-correction (Sitzenfrei et al., 2020; Chegini and Li, 2022) are proposed to alleviate the computational burden related with optimization procedures. Nevertheless, a trade-off between approximation-based solution quality and computational efficiency still exists for large-scale cases (Yu et al., 2024).

Considering previous achievements in VND, this study further proposes a Virtual Network Reconstruction (VNR) approach to improve the physical realism of sewer representations in urban pluvial flood simulation. While VND optimizes network design for economic cost and drainage performance, VNR estimates the most possible network properties constrained by partially known information. Although existing tools such as SWMManywhere (Dobson et al., 2025) have offered practical solutions for high-quality VND using publicly available datasets, certain discrepancies between virtual and real networks still inevitably exist due to inherent assumptions and simplifications, such as predefined road alignments for network topology, river proximity for outfall location, and ideal hydraulic design using the Rational Method. These discrepancies can potentially alter hydrological connectivity and lead to undesirable performance in flood simulation (Tran et al., 2024). Thus, in order to enhance the physical realism of virtual networks, additional efforts should be devoted to incorporating partially known information as constraints of network generation. This leads to a critical challenge: while basic network attributes like terminal nodes, spatial layout, and pipe sizes can be possibly identified and easily adjusted through existing VND toolsets, field surveys and engineering drawings, key hydraulic parameters such as flow directions and invert elevations often remain unknown or hard to achieve efficient estimation at city scale. To bridge this gap, we present our VNR approach that integrates partial network information with surface elevation data to derive the most possible hydraulic parameters, thereby reducing simulation uncertainty of sewer drainage effects in urban flood modeling.

In the remainder of this paper, we first describe the proposed workflow for VNR (Sect. 2) along with the corresponding 1D/2D coupled hydrologic-hydrodynamic model for urban pluvial flood simulation (Sect. 3) and then conduct a comparative analysis of flood simulation performance under varying levels of information completeness during reconstruction, taking into account factors such as regulated facility removal and road-based layout simplification (Sect. 4).

75 2 Graph-based sewer network reconstruction

2.1 Graph representation of sewer networks

The necessary inputs of sewer network reconstruction include the sewer network layout with specified outfalls and corresponding digital elevation model (DEM). For convenience of topological analysis, we represent the sewer network as an undirected graph G = (V, E) where $V = \{v_i\}$ and $E = \{e_{i,j}\}$ represent the sets of nodes and links, respectively (Shi et al., 2023). Then we can specify the link directions as related gravitational flow directions and convert the original undirected graph to the corresponding directed form $G_D = (V, E_D)$ where $E_D = \{\overrightarrow{e}_{i,j}\}$ represents the set of directed links evaluated as follows:

$$\overrightarrow{e}_{i,j} = \begin{cases} 1, & v_j \in \mathcal{N}_{G_D}(v_i) \\ 0, & v_j \notin \mathcal{N}_{G_D}(v_i) \end{cases}, \forall v_j \in \mathcal{N}_G(v_i)$$
 (1)

where $\mathcal{N}_{G_D}(v_i)$ and $\mathcal{N}_G(v_i)$ represent the neighboring nodes of node v_j in G_D and G.

For one node v_i , its out-degree $d_{\text{out},i}$ and in-degree $d_{\text{in},i}$ can be defined as the number of directed links pointed from/to it:

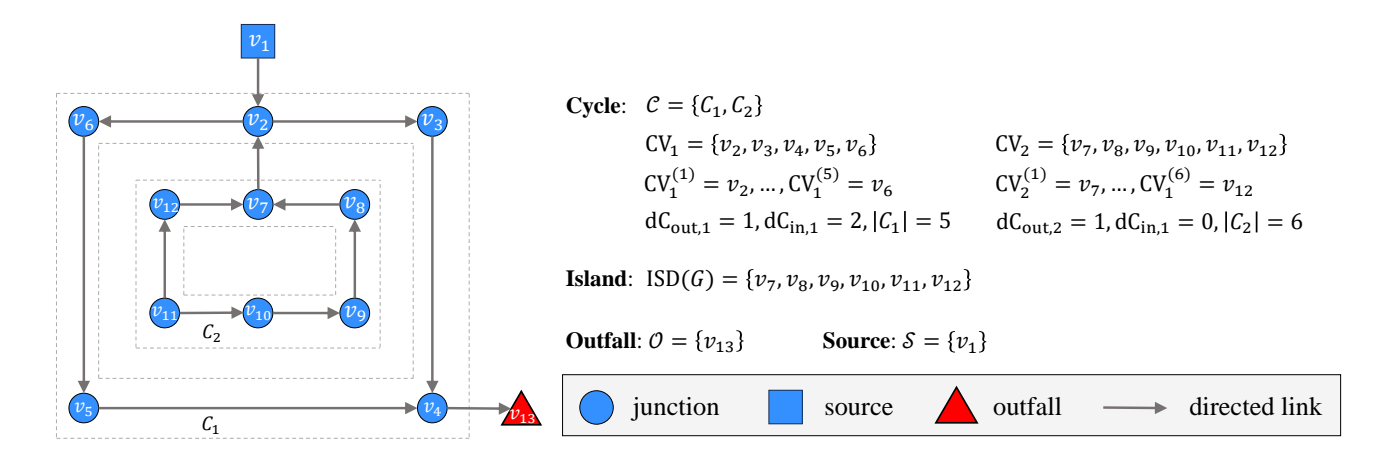


Figure 1. Cycles, islands, outfalls and sources in the graph-based sewer network representation.

85
$$d_{\text{out},i} = \sum_{v_j \in \mathcal{N}_G(v_i)} \overrightarrow{e}_{i,j}, d_{\text{in},i} = \sum_{v_j \in \mathcal{N}_G(v_i)} \overrightarrow{e}_{j,i},$$
 (2)

In addition to these basic attributes, some useful structures can be derived from the graph representation. Considering the potential cycles in the geometric layout of G, we identify the set of simple cycles $\mathcal{C} = \{C_k\}$ defined as the set of closed paths where no node appears twice (Johnson, 1975), such as C_1 and C_2 in Fig. 1. For a cycle $C_k \in \mathcal{C}$, we group its internal nodes into the corresponding set denoted by CV_k where the i-th node is indexed by $\mathrm{CV}_k^{(i)}$. Then its out-degree $\mathrm{dC}_{\mathrm{out},k}$ and in-degree $\mathrm{dC}_{\mathrm{in},k}$ can be defined as follows:

$$dC_{\text{out},k} = \sum_{v_i \in \text{CV}_k} \sum_{v_j \in \mathcal{N}_G(v_i) \backslash \text{CV}_k} \overrightarrow{e}_{i,j}, dC_{\text{in},k} = \sum_{v_i \in \text{CV}_k} \sum_{v_j \in \mathcal{N}_G(v_i) \backslash \text{CV}_k} \overrightarrow{e}_{j,i}$$
(3)

where $\mathcal{N}_G(v_i)\backslash \mathrm{CV}_k$ represents the difference set between $\mathcal{N}_G(v_i)$ and CV_k , i.e., the set of nodes that are neighboring nodes of v_i but not in C_k .

According to Eq. 3, we define a cycle C_k as an "island" if the sum of its in-degree and out-degree is equal to 1, such as C_2 in Fig. 1. We further denote the set of nodes located in the islands of G as ISD(G):

$$ISD(G) = \bigcup_{C_k} CV_k \quad \text{s.t.} \quad dC_{\text{out},k} + dC_{\text{in},k} = 1$$
(4)

In addition to general properties, we also consider some sewer-related hydraulic characteristics for the convenience of the following analysis. For a node $v_i \in V$, we include it in the set of outfalls (denoted as \mathcal{O}) if its out-degree is 0 and in-degree is 1, such as v_{13} in Fig. 1, or in the set of sources (denoted as \mathcal{S}) if its in-degree is 0 and out-degree is 1, such as v_1 in Fig. 1:

100
$$\mathcal{O} = \{ v_i \mid v_i \in V, d_{\text{out},i} = 0, d_{\text{in},i} = 1 \}, \mathcal{S} = \{ v_i \mid v_i \in V, d_{\text{out},i} = 1, d_{\text{in},i} = 0 \}$$
 (5)

During practical usage, the set of sources can be derived as the difference set between the set of predefined outfalls and the set of nodes whose in-degree and out-degree are summed to 1.

To allow for hydraulic simulation, we also attach the invert elevation attribute to v_i (denoted as z_i) which can be initialized as follows:

105
$$z_i^{(0)} = z_{q,i} - D_{\min}$$
 (6)

where $z_i^{(0)}$ is the initial value of z_i ; $z_{g,i}$ is the surface elevation at the location of v_i ; D_{\min} is the minimum allowable cover depth and set as $D_{\min} = 0.6$ m by default (MOHURD, 2021).

By comparing invert elevations of neighboring nodes, link directions can be initialized as follows:

$$\overrightarrow{e}_{i,j}^{(0)} = \begin{cases} 1, & z_i^{(0)} \ge z_j^{(0)} \\ 0, & z_i^{(0)} < z_j^{(0)} \end{cases}$$
(7)

110 2.2 Gravitational flow direction derivation

Since flow direction initialization using Eq. 7 does not consider the necessary topological constraints for a feasible layout of the sewer network (Fig. 2), it may produce an unfeasible or unreasonable layout and therefore needs further correction (Reyes-Silva et al., 2023).

In order to maintain flow directions as intact as possible during correction, we formulate the following 0-1 programming problems with linear constraints summarized in Table 1:

$$\min_{e_{ij}} \sum_{\overrightarrow{e}_{i,j}} \left| \overrightarrow{e}_{i,j} - \overrightarrow{e}_{i,j}^{(0)} \right| \tag{8}$$

Prior to optimization, pipes are discretized into 50 m segments following common inlet spacing (MOHURD, 2021). This ensures uniform link lengths for objective evaluation and provides computational elements with inlets at endpoints for surface-sewer exchange in hydraulic simulation.

120 2.3 Nodal invert elevation derivation

Corrected gravitational flow directions pave the way for the derivation of nodal invert elevation prepared for downstream hydraulic simulation. Based on invert elevation initialized by Eq. 6, further adjustment is needed to keep the slopes of links within the range of minimum and maximum allowable slopes (Safavi and Geranmehr, 2017).

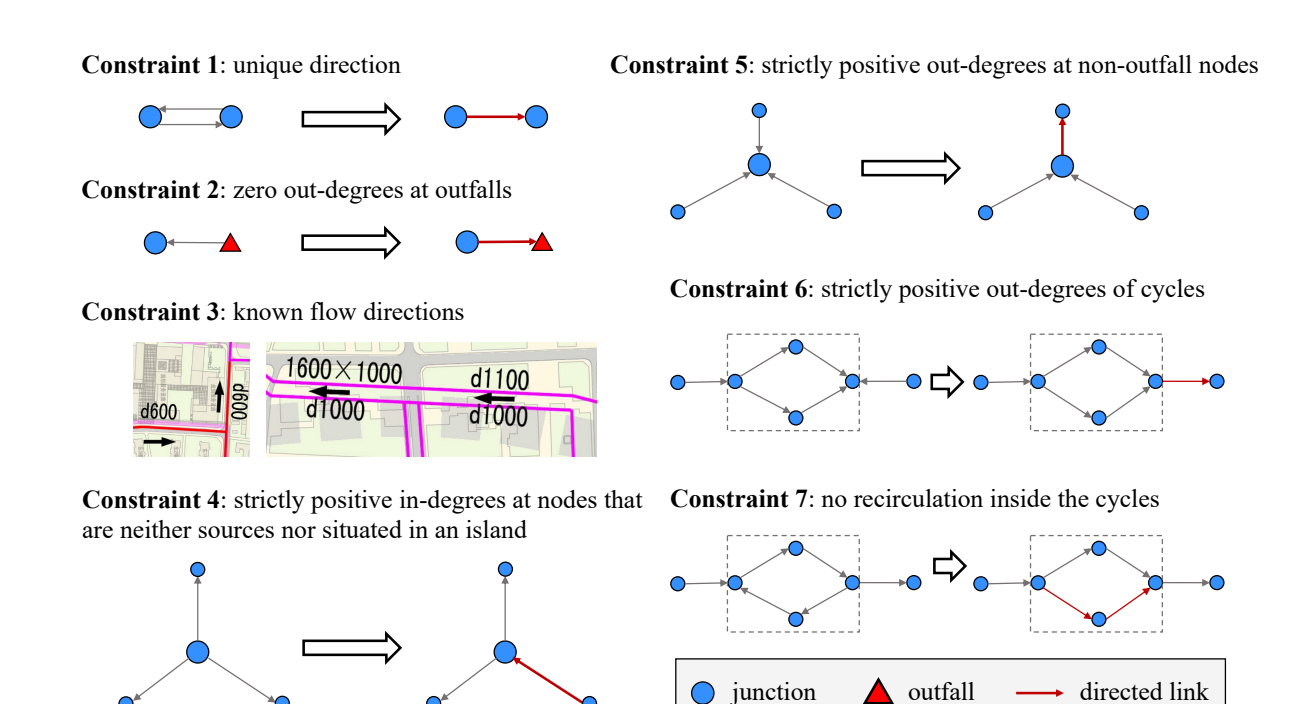


Figure 2. Topological constraints for a feasible sewer network.

Table 1. Optimization constraints of gravitational flow direction derivation. $|C_k|$ is the number of nodes in C_k ; \mathcal{E}_D^* is the set of links with known directions (denoted by $\overrightarrow{e}_{i,j}^*$); $\overrightarrow{e}_{\mathrm{CV}_k^{(|\mathcal{C}_k|)},\mathrm{CV}_k^{(1)}} + \sum_{i=1}^{|\mathcal{C}_k|-1} \overrightarrow{e}_{\mathrm{CV}_k^{(i)},\mathrm{CV}_k^{(i+1)}}$ is the sum of consecutively connected direction values along C_k .

Constraint	Description
$\overrightarrow{e}_{i,j} = 1 - \overrightarrow{e}_{j,i}$	No bi-directional links between consecutive nodes
$\overrightarrow{e'}_{i,j} = 1, orall v_j \in \mathcal{O}$	Outfalls must have zero out-degree
$\overrightarrow{e}_{i,j} = \overrightarrow{e}_{i,j}^*, orall \overrightarrow{e}_{i,j} \in \mathcal{E}_D^*$	Preserves known link directions
$d_{\mathrm{in},i} \ge 1, \forall v_i \notin \mathcal{S} \cup \mathrm{ISD}(G)$	Nodes except for sources and those located in the islands
	must have positive in-degrees (Eq. 4)
$d_{\mathrm{out},i} \geq 1, \forall v_i \notin \mathcal{O}$	Nodes except for outfalls must have positive out-degrees
$dC_{\mathrm{out},k} \ge 1, \forall C_k \in \mathcal{C}$	Cycles must have positive out-degrees for flow passage
$\overrightarrow{e}_{\text{CV}_{k}^{(C_{k})},\text{CV}_{k}^{(1)}} + \sum_{i=1}^{ C_{k} -1} \overrightarrow{e}_{\text{CV}_{k}^{(i)},\text{CV}_{k}^{(i+1)}} \le C_{k} - 1, \forall C_{k} \in \mathcal{C}$	No recirculation within cycles

In order to achieve the least deviation from initial results considering sewer construction costs proportional to excavation depth (Swamee and Sharma, 2013; Machine Hsie and Huang, 2019), we introduce the following nonlinear optimization problem to estimate the invert elevation of nodes:

$$\min_{z_i} \sum_{z_i} \left| z_i - z_i^{(0)} \right|$$
s.t.
$$\begin{cases}
i_{i,j} \le -i_{\min,i,j}, & \forall \overrightarrow{e}_{i,j} = 1 \\
i_{i,j} \ge -i_{\max,i,j}, & \forall \overrightarrow{e}_{i,j} = 1
\end{cases}$$
(9)

where $i_{i,j}$ is the slope of $\overrightarrow{e}_{i,j}$; $i_{\min,i,j}$, $i_{\max,i,j}$ are the minimum and maximum allowable slopes of $\overrightarrow{e}_{i,j}$ summarized from the Standard for Design of Outdoor Wastewater Engineering (MOHURD, 2021), considering both explicitly stated slope limits and those derived from velocity constraints (Swamee and Sharma, 2013).

For simplicity but without loss of generality, $i_{i,j}$ is estimated using the invert elevation of two consecutive nodes, ensuring the linearity of constraints for the above optimization problem:

$$i_{i,j} = -\frac{1}{d_{i,j}} z_i + \frac{1}{d_{i,j}} z_j \tag{10}$$

It should be also noted that Eq. 10 can be also extended to the case of multiple consecutive nodes and corresponding slope estimator still remains in the form of the linear combination of nodal invert elevation (see Sect. S1 in the Supplementary Material), which maintains the linearity of constraints in the original optimization problem.

Table 2. Slope constraints with respect to different sizes according to Standard for Design of Outdoor Wastewater Engineering (MOHURD, 2021).

Diameter [mm]	Minimum slope	Maximum slope
300	0.002	0.41
400	0.0015	0.28
500	0.0012	0.21
600	0.001	0.16
800	0.0008	0.11
1000	0.0006	0.08
1200	0.0006	0.06
1400	0.0005	0.05
> 1500	0.0005	0.05

2.4 Computational efficiency considerations

The objective functions of Eq. 8 and Eq. 9 are expressed as the sum of absolute deviations and can be further reduced into an equivalent linear form as follows (Wagner, 1959; Giangrande et al., 2013), thus ensuring their solution efficiency for large-scale applications.

Without loss of generality, for minimizing the summation of absolute values:

$$L = \sum_{i=1}^{N} |k_i x_i - b_i| \tag{11}$$

where k_i, b_i are fixed numbers with respect to N decision variables x_i , we can introduce auxiliary decision variables $z_i = |k_i x_i - b_i|$ constrained by:

$$\begin{cases}
z_i \ge k_i x_i - b_i \\
z_i \ge -k_i x_i + b_i \\
z_i \ge 0
\end{cases} \tag{12}$$

Thus, the original unconstrained nonlinear problem can be reformulated into an equivalent linear one with additional constraints:

$$\min_{x_{i}, z_{i}} \sum_{i=1}^{N} z_{i}$$
s.t.
$$\begin{cases}
z_{1} \ge k_{i}x_{1} - b_{0}, z_{1} \ge -k_{i}x_{1} + b_{0}, z_{1} \ge 0 \\
\dots, \dots \\
z_{N} \ge k_{i}x_{N} - b_{N}, z_{N} \ge -k_{i}x_{N} + b_{N}, z_{N} \ge 0
\end{cases}$$
(13)

Furthermore, if additional constraints are present with Eq. 11, they can be added directly to the reformulated problem (Eq. 13) without loss of equivalence. This reformulation strategy has been used in previous research (Giangrande et al., 2013) and thus can be easily extended to our work for efficient sewer network reconstruction (Eq. 8 and Eq. 9). In terms of solving the reformulated linear programming problems, we select the open-source Computational Infrastructure for Operations Research (COIN-OR) branch-and-cut solver (CBC) (Forrest and Lougee-Heimer, 2005) through its Python interface in PuLP (Mitchell et al., 2011).

155 3 AUTOSHED: A 1D/2D coupled hydrologic-hydrodynamic model

Given the sewer network reconstructed from incomplete information, we further adopt a 1D/2D coupled hydrologic-hydrodynamic model named AUTOSHED to simulate the pluvial flood process in the urbanized area. AUTOSHED delineates the whole simulation domain into multiple triangular-shaped units (TSUs). For each unit, AUTOSHED uses the Rain-on-Grid approach, also known as the Fully Hydrodynamic Approach (Hall, 2015; Chen and Huang, 2024; Perrini et al., 2024), and performs sequential hydrologic-hydrodyamic computations for surface runoff generation and routing, respectively.

3.1 Surface runoff generation and routing

The surface runoff generation scheme is mainly built upon the core module of the Surface Urban Energy and Water Balance Scheme (SUEWS) (Järvi et al., 2011) and Tsinghua Integrated Hydrological Modeling System (THIHMS) (Ni et al., 2008) except for overland and channel flow routing. Each TSU is divided into impervious and pervious parts according to the empirical impervious ratio $\alpha_{\rm imp}$ derived from the unit land use statistic by area-weighted averaging (Cao et al., 2020; Krebs et al., 2014). And the total surface runoff $\Delta S_{\rm sr}$ is calculated as the area-weighted sum of runoff from the impervious and pervious parts considering typical hydrological processes such as vegetation interception, building interception and soil infiltration (Fig. 3). Details of methodologies for rainfall-runoff simulation can be found in the work of (Ni et al., 2008) and (Järvi et al., 2011). After obtaining total surface runoff, a well-balanced formulation of 2D shallow water equations (SWEs) (Song et al., 2011) is adopted to simulate the subsequent surface routing process:

$$\frac{\partial}{\partial t} \begin{bmatrix} h \\ hu \\ hv \end{bmatrix} + \frac{\partial}{\partial x} \begin{bmatrix} hu \\ hu^2 + g(h^2 - z_b^2)/2 \\ huv \end{bmatrix} + \frac{\partial}{\partial y} \begin{bmatrix} hu \\ huv \\ hv^2 + g(h^2 - z_b^2)/2 \end{bmatrix} = \begin{bmatrix} \Delta S_{sr} - q_{sd} \\ -g(h+z_b)\frac{\partial z_b}{\partial x} - gh\frac{n^2u\sqrt{u^2 + v^2}}{h^{4/3}} \\ -g(h+z_b)\frac{\partial z_b}{\partial y} - gh\frac{n^2v\sqrt{u^2 + v^2}}{h^{4/3}} \end{bmatrix}$$
(14)

where h is the water depth; u, v are the depth-averaged velocity components in the x- and y-directions; z_b is the bed elevation; g is the gravitational acceleration; $q_{\rm sd}$ is the mass loss term caused by sewer drainage; n is the empirical Manning coefficient initialized as n_0 by land use types and further increased according to the intersected area ratio of TSUs with buildings (denoted as b_f) by the building roughness method (Schubert and Sanders, 2012) where the maximum roughness is set as $0.5 \text{ s/m}^{1/3}$. Details of methodologies for solving 2D SWEs can be found in the work of Song et al. (2011).

3.2 Sewer flow simulation

170

175

In the TSU with rainwater inlets, vertical linkages are established for bidirectional coupling between the surface flow and the sewer flow. A modified form of the 1D Saint-Venant equations is introduced to simulate the sewer flow process using a node-link approach (Rossman and Huber, 2017):

$$\begin{cases}
\frac{\partial H}{\partial t} = \frac{Q_{1D-2D} + \sum Q_{nl}}{A_{as}} \\
\frac{\partial Q}{\partial t} = 2U\frac{\partial A}{\partial t} + U^2\frac{\partial A}{\partial x} - gA\frac{\partial H}{\partial x} - gAS_f
\end{cases}$$
(15)

where H is the total nodal hydraulic head of water; Q is the flow rate; U is the flow velocity; A is the cross-sectional area; $A_{\rm as}$ is the node assembly surface area consisting of node's storage surface area and half the surface area of connected links (Rossman, 2015); S_f is the friction slope parameterized by the Manning formula; $Q_{\rm nl}$ are the flow contributed by neighboring links in the sewer system; $Q_{\rm 1D-2D}$ is the mass source term exchanged between the surface flow and the sewer flow. Details of methodologies for solving 1D Saint-Venant equations under regulation can be found in Rossman (2015) and corresponding surface-sewer flow coupling scheme is given in the Sect. S2 in the Supplementary Material.

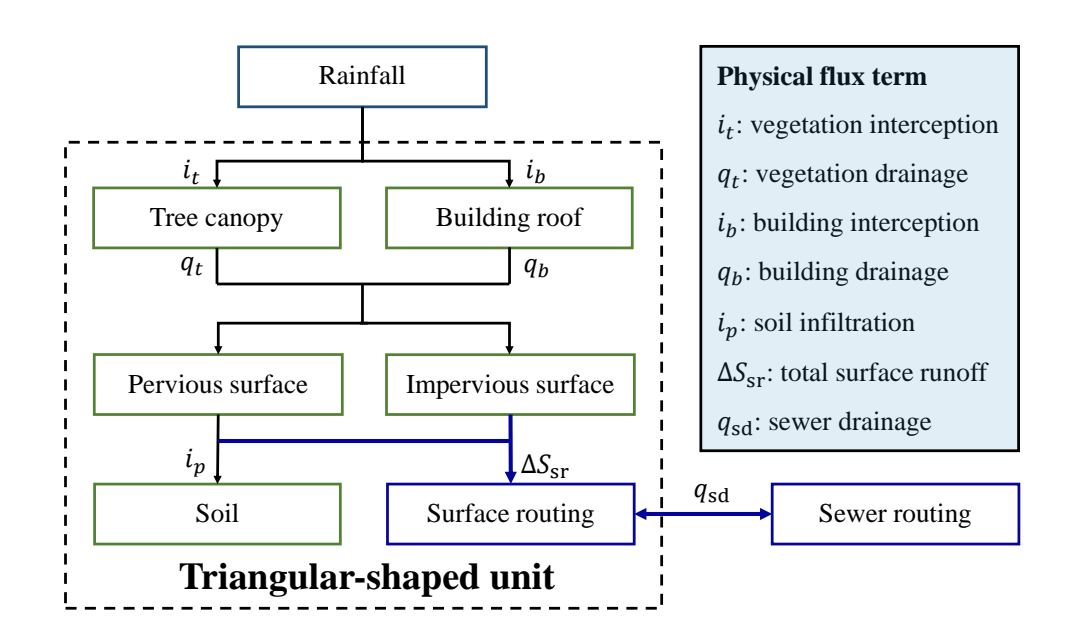


Figure 3. Flux calculation within a typical triangular-shaped unit and between surface-sewer system

4 Performance Analysis: From Graph Reconstruction to Urban Flood Simulation

4.1 Study area and data

200

The study area is the main city zone of Yinchuan (CYC), Ningxia Hui autonomous region, situated in the northwestern part of China, covering an area of 137.15 km². Desipte being located in an arid region with an average annual rainfall of 189 mm and annual evaporation of 1825 mm, CYC has experienced several flood disasters due to increasing extreme rainfall events in recent years (Lu et al., 2024). According to local documents, most of the drainage system in CYC is the combined sewer system, and therefore its drainage capacity is largely constrained by downstream wastewater treatment plants (WTPs) due to restrictive environmental regulations, which may result in overflow at rainwater inlets and further amplify the surface inundation risks.

In order to establish the urban pluvial flood model for scenario analysis, we collect multi-source geographical datasets listed as follows:

- 5 m digital elevation model (DEM, Fig. 4 (a)) generated from the stereo images of ZiYuan-3 satellite. Following common practices of DEM preprocessing in urban flood simulation, we delete the inaccurately measured building roof elevation from the original product (Chen and Huang, 2024) and lower the surface elevation of grids containing roads by 0.2 m (Liu et al., 2022) to improve the representation of hydrological connectivity in DEM.
- 10 m land use map (Fig. 4 (b)) collected from the European Space Agency (ESA) WorldCover 2021 product (Zanaga et al., 2022) and covers tree, grassland, cropland, built-up and bareland area in the study area.

- Building footprint (Fig. 4 (a)) and road network layers (Fig. 4 (b)) downloaded via the application programming interface
 of the Baidu map. Considering potential underestimation of impervious area identified from remote sensing datasets
 (Weng, 2012), we further modify the land use type as built-up area at pixels intersected with buildings and roads.
 - Sewer network layout and corresponding attribute of pipeline sizes (Fig. 5 (a)) digitized from investigation and design documents authorized by the local government. It should be noted that when detailed information is unavailable, previous research would generate a virtual sewer network from the street network (Montalvo et al., 2024). In order to investigate potential effects induced by such simplification, we further create a road-based sewer network by identifying pipes intersected with the major roadway zone and then performing necessary reconnections at pipes broken intermediately (Fig. 5 (b)). Here we define the term of "major road" (Fig. 4 (b)) as the union of the primary, secondary, tertiary and trunk roads and then generate corresponding roadway zones by buffering road centerlines with the width evaluated from The Design of Urban Road Engineering (CJJ 37—2012).

The formula of the designed rainfall in CYC is also collected based on local rainfall statistics:

$$q = \frac{551.4(1+0.584\lg P)}{(t+11)^{0.669}} \tag{16}$$

where q is the rainfall intensity, L/(s · ha); P is the return period; t is the rainfall duration, min.

Seven designed rainfalls with return years of 1a, 5a, 10a, 20a, 50a, 100a, and 200a are selected for the scenario analysis where each rainfall event lasts for 2 h (see Fig. S1 in the Supplementary Material), followed by an additional 2 h period without any precipitation.

4.2 Baseline configurations

210

220

225

230

Five baselines are selected for the comparison of the performance between the proposed approach (denoted as the FSR approach) and other approximation methods:

- Full-Sewer-reconstruction-No-controls (FSN) which uses the same reconstruction approach but ignores the existence of regulated facilities such as pump stations and wastewater treatment plants. To be specific, regulated facilities located at outflow and intermediate points are configured as free outfalls and uncontrolled junctions, respectively.
- Road-based-Sewer-reconstruction-No-controls (RSN) which uses the same reconstruction approach but adopts the layout
 of sewers filtered by the major roadway zone (Fig. 5 (b)) and ignores the existence of regulated facilities.
- Road-based-Sewer-reconstruction-with-Controls (RSC) which uses the reconstructed sewer network from RSN and further incorporates regulated facilities at corresponding locations.
 - Road-Drainage Approximation (RDA) (Xing et al., 2021; Li et al., 2023) which subtracts the mass at a uniform rate i_d from the roadway zone buffered from road centerlines using widths evaluated by The Design of Urban Road Engineering (CJJ 37—2012).

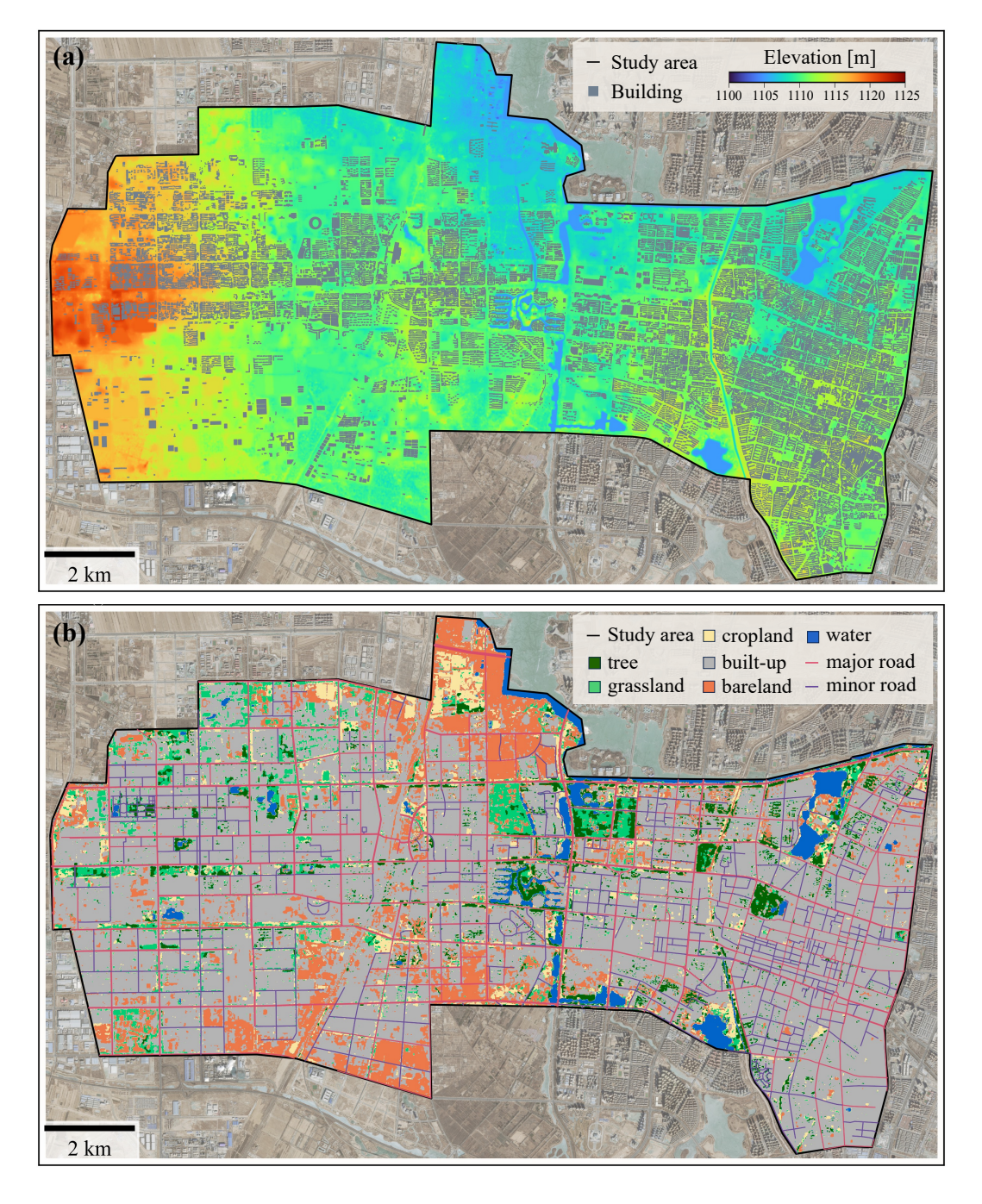


Figure 4. Geographical datasets in the study area. (a) Digital elevation model. (b) Land use map and road networks. Basemaps are derived from ESRI World Imagery (Credit: Esri, TomTom, Garmin, FAO, NOAA, USGS, © OpenStreetMap contributors, and the GIS User Community).

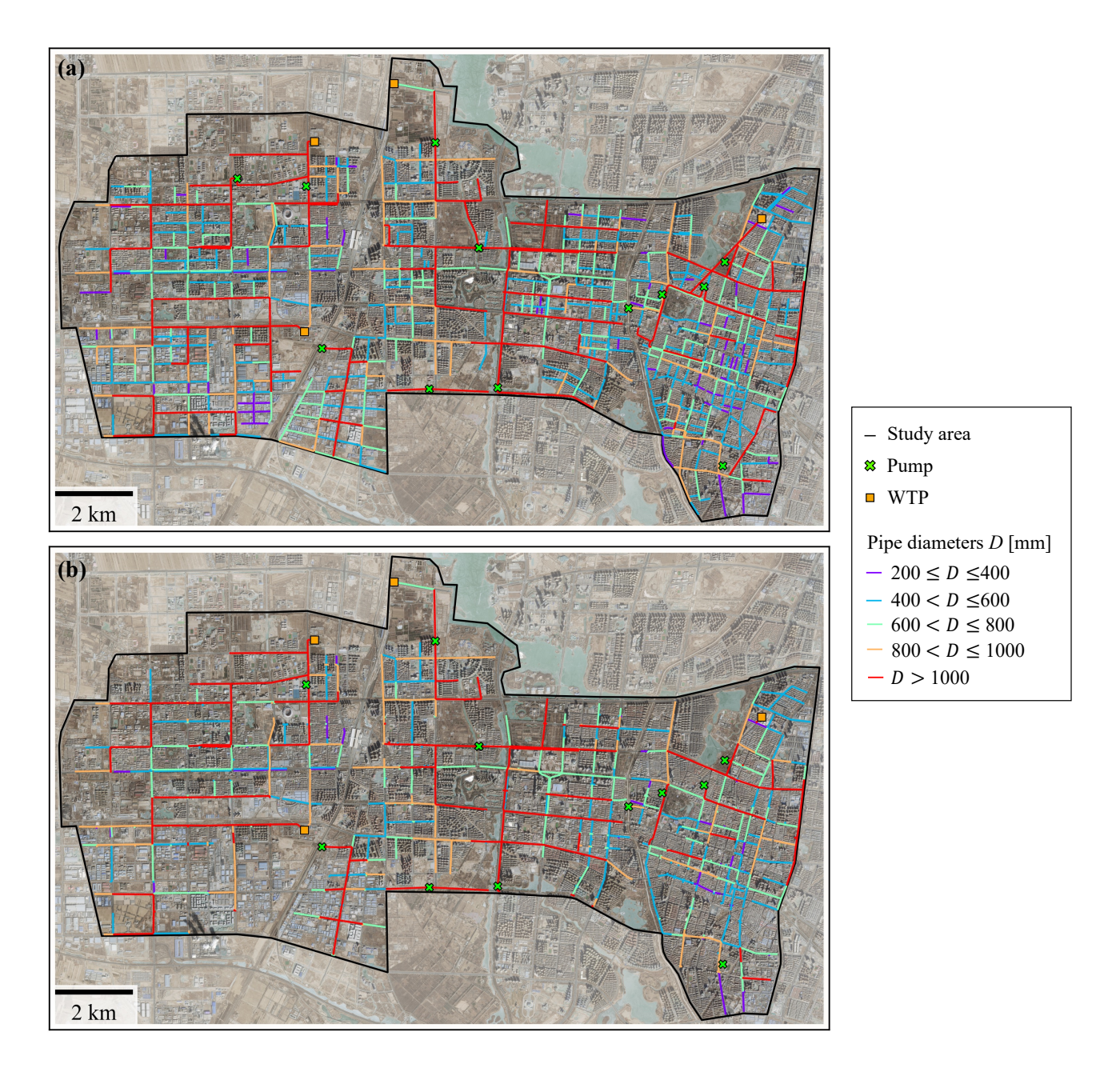


Figure 5. Sewer network in the study area. (a) Complete sewer network digitized from the local document. (b) Simplified sewer network filtered within major roadway zone. Basemaps are derived from ESRI World Imagery (Credit: Esri, TomTom, Garmin, FAO, NOAA, USGS, © OpenStreetMap contributors, and the GIS User Community).

- No-Drainage Approximation (NDA) which ignores the drainage effects of the sewer network.

According to whether a sewer hydraulic module is reconstructed for simulation with AUTOSHED, we can further classify the above approximation methods into two categories: physical approaches (including FSR, FSN, RSN and RSC), and equifinal ones (including RDA and NDA), meaning similar flood simulation results can be achieved by different methods with appropriate parameters of drainage effects (Dobson et al., 2025).

In order to quantify the simulation performance of different approximation methods under design scenarios, we select the Probability of Detection (POD), False Alarm Rate (FAR), Critical Success Index (CSI) and Bias (BIAS) of inundation area simulations (McGrath et al., 2018), using results from the FSR approach as the reference (see Sect. S3 in the Supplementary Material).

4.3 Sewer network reconstruction performance

245

250

255

260

265

According to the layout of the digitized sewer network (Fig. 5), gravitational flow directions are initialized by surface elevation (Eq. 7) and then estimated by solving 0-1 programming problems (Eq. 8). For simplicity, Fig. 6 summarizes the corresponding results for the initialized and reconstructed directions of the complete sewer network with 11 outfall points consisting of wastewater treatment plants and pumping stations. The directions of 359 in 908 pipes are reversed to satisfy the topological constraints. The majority of modified pipes are located in the southern part of the study area and exhibit a pattern of cyclic structures over a relatively flat areas, posing challenges on the direct identification of dominant flow directions and thus necessitating the incorporation of additional topological constraints (Table 1) for rational reconstruction.

According to reconstructed flow directions, nodal invert elevation is further derived from values initialized by a constant cover depth (Eq. 6) and the slope distributions before / after adjustment are summarized in Fig. 7. The initial slopes of both complete and simplified sewer network exhibit a relatively symmetric distribution centered on 0, indicating adverse slopes in nearly half a number of links due to nearly reversed 40% pipes in the previous step. After reconstruction using Eq. 9, slope distributions are shifted into strictly positive ones where the majority of slopes are around 0.001. Additionally, the simplified sewer network shares a similar pattern in the slope distribution with the complete one except for minor increases around 0 because its layout is slightly modified due to aforementioned reconnection of broken pipes in Sect. 4.1. Thus, it can be concluded that the proposed reconstruction approach is robust to empirical simplification of the sewer network layout following road networks and can be stably extended to cases using street-based network generation.

Owing to linearized programming formulation used in the process of gravitational flow directions and nodal invert elevation reconstruction (Sect. 2.4), 1D sewer hydraulic models can be built from prepared geographical datasets in 33 seconds on a local desktop using a single core of Intel(R) Core(TM) i7-14700KF CPU and 400 MB RAM occupancy. According to reconstructed sewer networks initialized with a uniform spacing of 50 m (cf. Sect. 2.2), FSR/FSN and RSN/RSC models have 8242 links and 8131 inlets, 5268 links and 5188 inlets, respectively. Furthermore, the entire study area is discretized into 7222150 TSUs with a median area of 18.2 m² for surface runoff generation and routing computation.

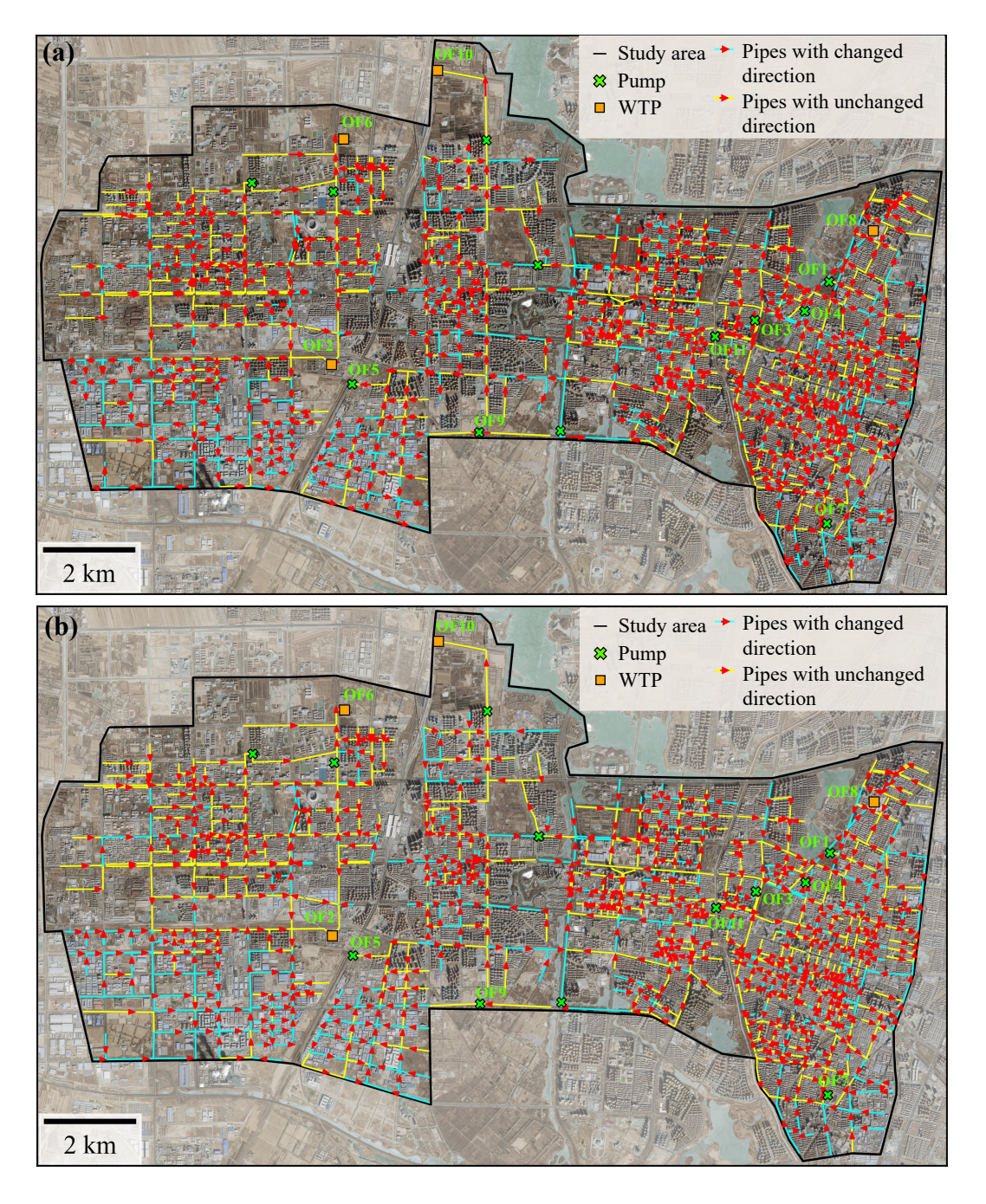


Figure 6. Comparison of initial and reconstructed gravitational flow directions of the complete sewer network in the study area. (a) Flow directions initialized by surface elevation. (b) Flow directions reconstructed from topological constraints. Basemaps are derived from ESRI World Imagery (Credit: Esri, TomTom, Garmin, FAO, NOAA, USGS, © OpenStreetMap contributors, and the GIS User Community).

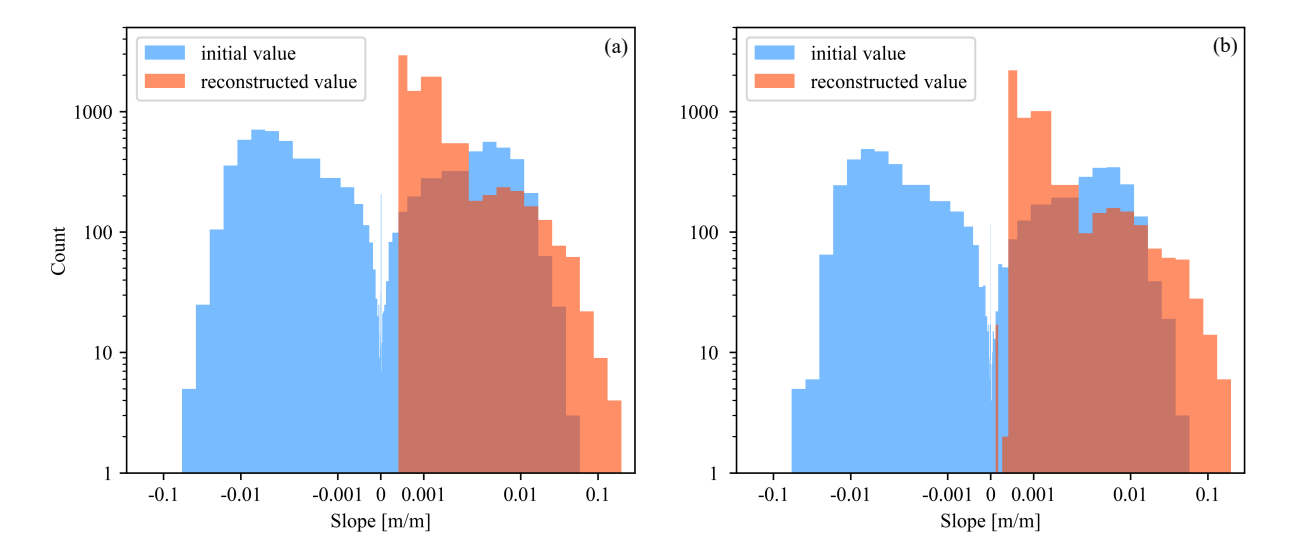


Figure 7. Comparison of initial and reconstructed sewer slope distributions. (a) Complete sewer network used in the FSR and FSN approaches. (b) Road-based sewer network used in the RSN and RSC approach.

4.4 Model calibration and evaluation

280

To facilitate the comparison of pluvial flood simulation performance using different approaches, we first calibrate the model parameters with a severe storm hitting CYC on 11 July 2022 (denoted as the July 2022 storm). This storm brings an average total rainfall of 57.8 mm and a peak intensity of 44.5 mm/h, resulting in 31 inundated points reported by the local government, of which 18 are recorded with corresponding maximum waterlogging depth. Considering its representativeness as disastrous torrential events and data availability, we use the information of recorded maximum waterlogging depth to calibrate the parameters in the aforementioned model and related approximation approaches for the sewer drainage effect.

For AUTOSHED, the main physical parameters include the empirical impervious ratio $\alpha_{\rm imp}$ and the Manning coefficient n estimated from land use types. Considering the dominance of the built-up area and attempts to avoid possible parameter equifinality between physical process such as soil infiltration and sewer drainage, we perform simple tests of model performance using recommended empirical values of corresponding parameters from the Technical Specification for Construction and Application of Mathematical Model of Urban Flooding Prevention and Control System (DB11/T 2074-2022) and finalize the values of parameters without exhaustive search (see Table. S1 in the Supplementary Material for details). Fig. 8 shows the inundation map simulated by AUTOSHED with the sewer hydraulic module reconstructed from the FSR approach under the July 2022 storm.

The coefficient of determination (\mathbb{R}^2) is used to quantify the overall performance of the models using different parameters. According to Fig. 9 (a), the FSR approach achieves an \mathbb{R}^2 of 0.95, which indicates good agreement between the simulated and observed values and thus consolidates the physical background for further comparison. In addition, we further examine the performance of the FSR approach with varying inlet spacings (denoted as ILS) from 30 m to 100 m. According to Fig. 9 (b),

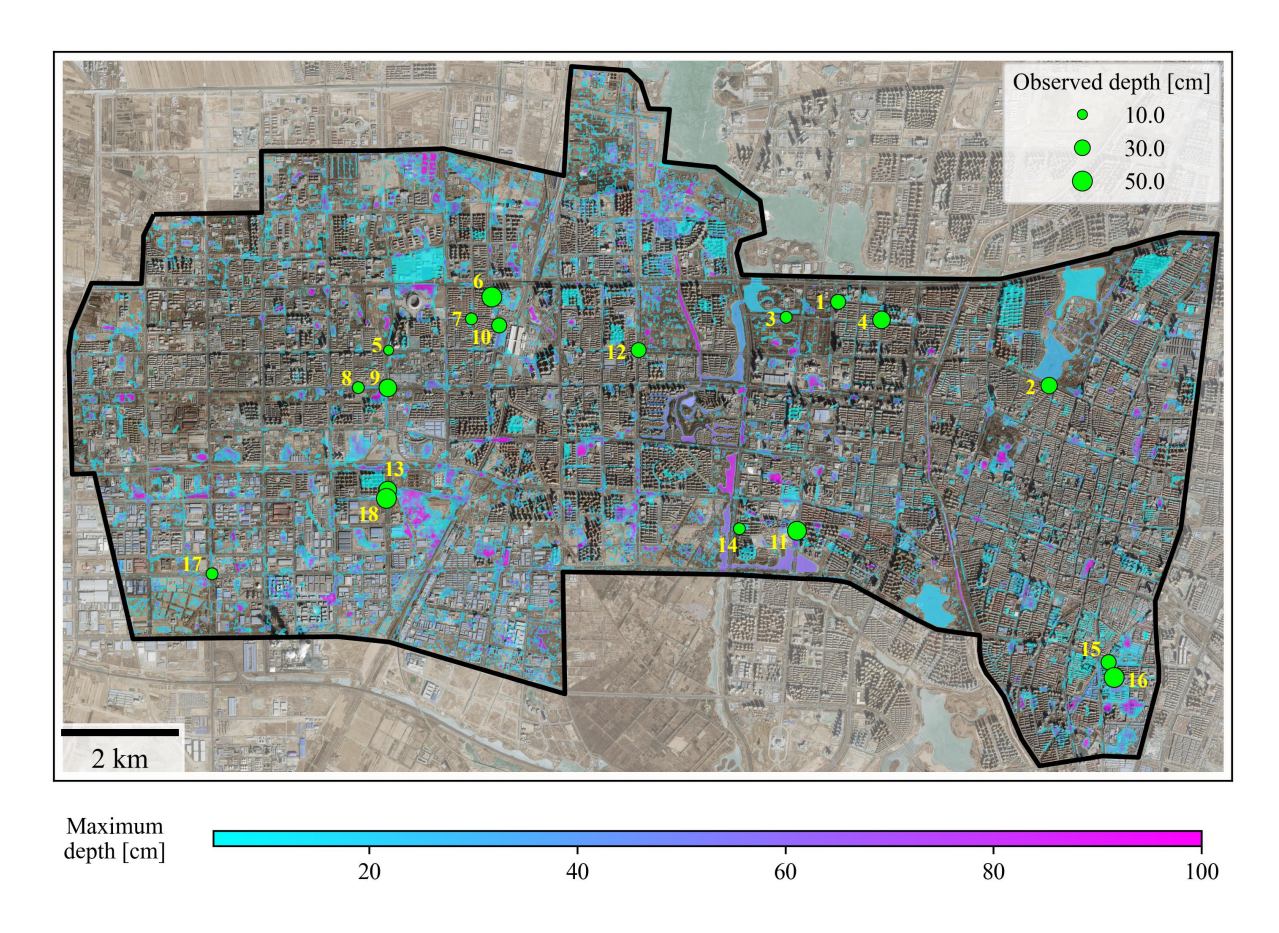


Figure 8. Maximum inundation depth map simulated by the FSR approach under the July 2022 storm. Basemaps are derived from ESRI World Imagery (Credit: Esri, TomTom, Garmin, FAO, NOAA, USGS, © OpenStreetMap contributors, and the GIS User Community).

the FSR approach demonstrates relatively robust performance with R² ranging from 0.85 to 0.95 where ILS of 50 m achieves the highest NSE. It is worth noting that increasing ILS leads to both underestimation and overestimation, such as P5 and P2 in Fig. 9 (b), highlighting the dual role of rainwater inlets in either alleviating surface inundation through drainage or contributing to it when overloaded.

Based on calibrated parameters of the physical model, we further use the grid search strategy to optimize the most possible equivalent drainage rate i_d used in the RDA method when detailed sewer network information is unavailable. Specifically, we set the possible range of i_d according to the local design drainage standard and perform simulations with i_d = 2.5, 5.0, 7.5, 10.0, 12.5, 15.0 mm/h. According to Fig. 9 (c), i_d = 2.5 mm/h achieves the highest R^2 and thus selected as the final value of drainage rate for further scenario analysis.

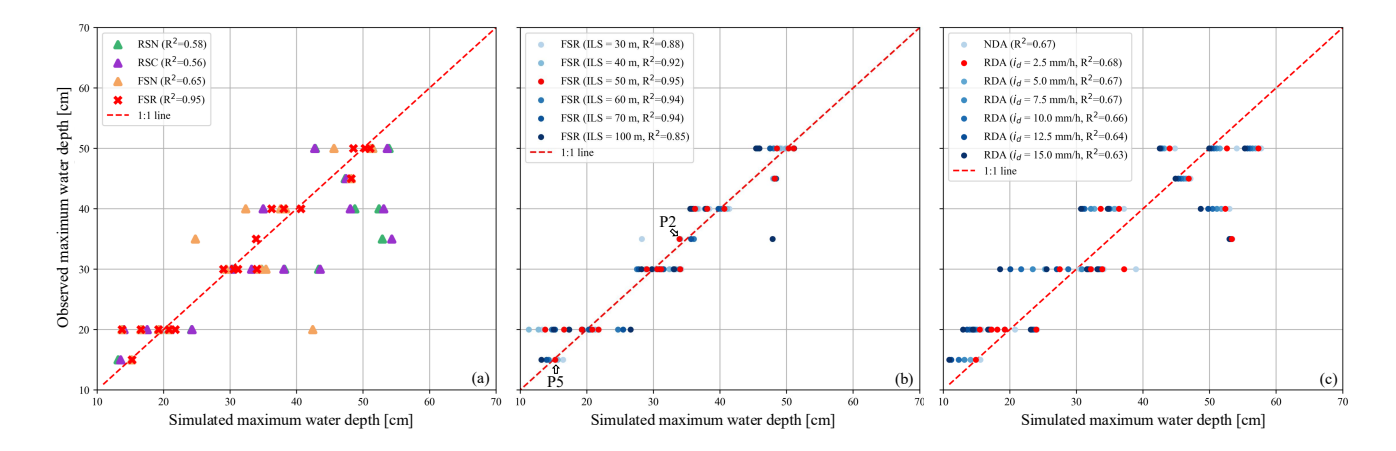


Figure 9. Simulation performance of the maximum inundation depth at inundated points using different approximation methods and parameters. The index of inundated points follow Fig. 8.

4.5 Extreme rainfall analysis: both local inlets and global regulation matter

305

310

After calibrating the AUTOSHED model integrated with reconstructed sewer hydraulic modules, we now delve deeper into understanding how the proposed graph reconstruction-based approach performs compared to simplified alternatives across different rainfall scenarios and varying levels of available information. The aforementioned July 2022 storm event, with an average total rainfall exceeding the 500-year return period threshold (40.8 mm), highlights its extremity in an arid region. According to Fig. 9, when information on regulated facilities and detailed layouts is unavailable, simplified physical approaches, such as FSN, RSC and RSN, exhibit relatively lower accuracy than calibrated equifinal ones, which approximate limited drainage capacities during extreme rainfall using a small equivalent drainage rate.

Considering physical approaches incorporate drainage effects at rainwater inlets, we further investigate the relationship between simulation error in maximum inundation depth and the distances to the nearest inlets, denoted as D_f for the complete sewer network and D_s for the simplified one (see Sect. 4.1), respectively. According to evaluation results (see Fig. S2 in the Supplementary Material), simulation error variability decreases as D_f and D_s increase, with the maximum absolute value of deviations remaining less than 5 cm for distances exceeding 30 m, where local microtopography predominantly influences the inundation. Furthermore, NDA can underestimate the maximum inundation depths at points such as P8 and P18, suggesting the occurrence of potential overflows surrounding nearby rainwater inlets due to insufficient drainage capacity under extreme rainfall.

To assess differences in simulated sewer drainage performance, we further summarize accumulated discharges at rainwater inlets and conduct two steps of comparisons according to available information.

- Effects of neglecting regulation: when neglecting the information of regulated facilities, FSN can significantly underestimate the maximum inundation depth at points such as P2 compared to FSR. This mainly results from overestimated inflows ($\Delta \sum Q_{\rm 1D-2D} > 0$) at surrounding inlets, as seen at P2 in Fig. 10 (a) and (e). Similar phenomenon of overestimated

tion can also be observed when comparing RSN with RSC whereas with greatly decreased magnitude since road-based simplification reduces the rainwater collected into the sewer system and thus alleviates the drainage burden. However, when regulated facilities are deleted, FSN can also overestimate the maximum inundation depths at certain points such as P1 and P3, which may seem counterintuitive. Analysis of P1's nearby inlets reveals lower inflows using FSN, compared to FSR, particularly at IL1 (Fig. 10 (b) and (f)), causing model overestimation of surrounding maximum inundation depth. After tracking accumulated discharges at downstream inlets with respect to IL1, we further locate the drainage bottleneck at one pump station PM1. As illustrated in Fig. 10 (d), its removal can significantly increase inflows at upstream inlets, further increasing water heads at adjacent sewer nodes and consequently reducing upstream inlet drainage capacities due to backwater effects.

315

320

325

330

345

- Impact of network simplification: when approximating the sewer layout through major roads, RSN generally overestimates the maximum water depths at inundated points within 30 m of rainwater inlets compared to FSN, driven by intensified overflows from excessive surface water flowing through a single drainage pathway, as seen at P1 in Fig. 11 (a) and (c). However, some inundated points like P13 and P18, where surrounding inlets are removed, may also exhibit underestimated maximum water depths. This occurs because these inlets initially contribute to surface overflows in FSN-based simulations, as evidenced by the underestimation of maximum water depth when NDA is adopted. In particular, we can also observe the overestimation of maximum water depths at certain flood points without removing local inlets during simplification, such as P2 and P4 with $\Delta D = 0$. Examining the simulated total discharges at rainwater inlets near P2 (Fig. 11 (b) and (d)) reveals that increased local inflows are outweighed by amplified upstream overflows, thus exacerbating downstream inundation conditions.

In summary, while physical approaches simplified through major roads can yield a similar pipe slope distribution (Sect. 4.3), achieving accurate simulation of maximum inundation depths still requires the proper configuration of regulated facilities and drainage pathways. Otherwise, equifinal methods, flexible in parameter calibration, can offer better performance, especially when observational data are available.

4.6 Design rainfall analysis: physical approaches outperform but require more complete information

In order to assess whether equifinal approaches always exhibit comparable or even better performance with physical counterparts, we further compare the inundated areas simulated by different approaches under design rainfalls where the FSR-based results serve as the reference.

In terms of detecting potential inundated areas, all approaches show only minor variations with high POD values ranging between 0.85 and 0.95. The NDA and RDA approaches even slightly outperform FSN, RSC and RSN under extreme rainfall conditions, aligning with previous results in Sect. 4.5. As rainfall return periods decrease, FAR values of the RSC, RSN, NDA and RDA approaches gradually increase, with the latter two showing much more significant variations. This indicates that the performance of the equivalent drainage rate i_d calibrated by a single event still has a high uncertainty when applied to rainfall scenarios with varying intensities. Therefore, while the differences in PODs are minimal, dramatically higher FARs

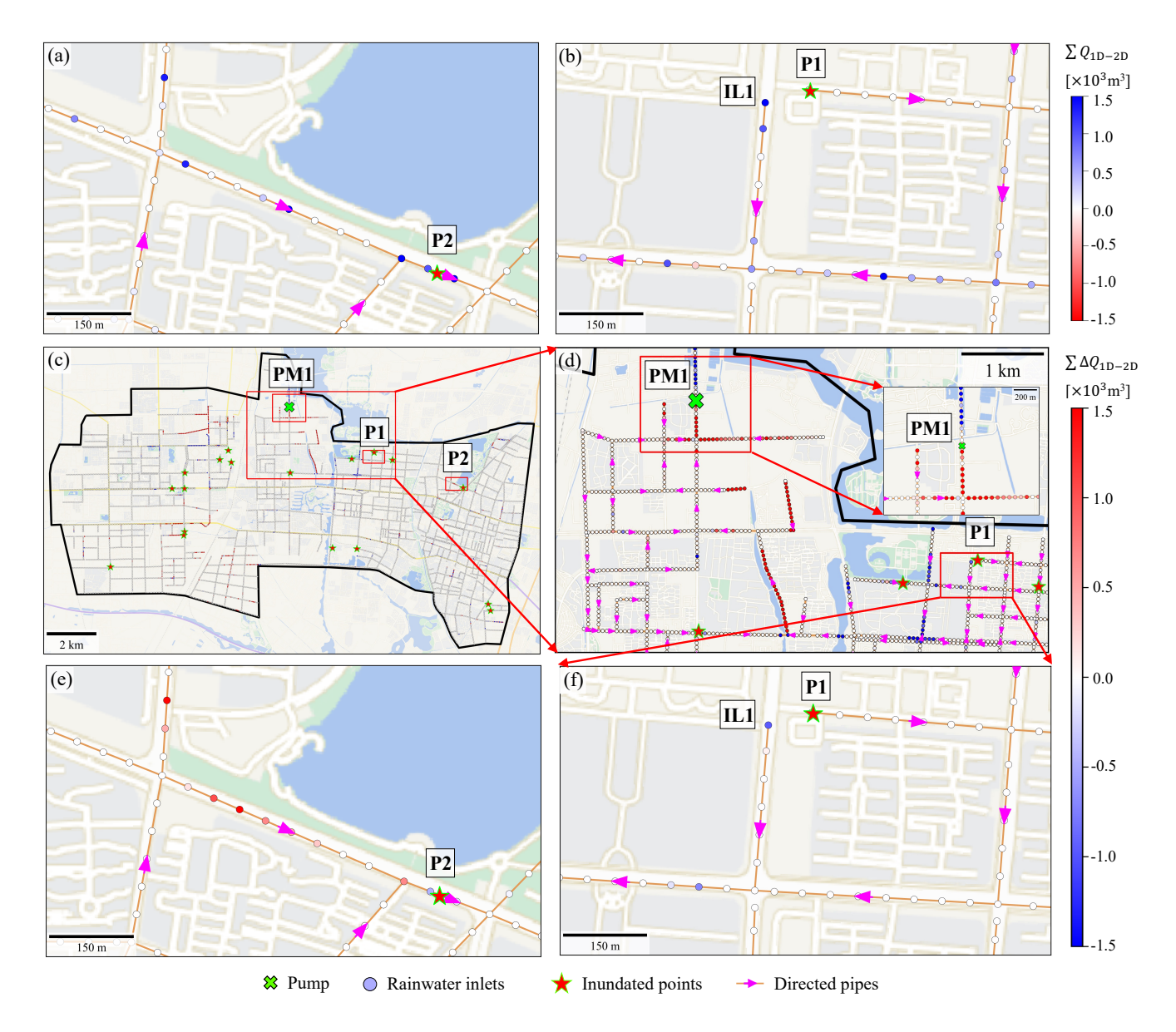


Figure 10. Comparison of accumulated discharges ($\sum Q_{\rm 1D-2D}$) at rainwater inlets during the July 2022 storm where positive values indicate inflows. (a)-(b). FSN simulated discharges. (c-f) Simulated discharge differences ($\sum \Delta Q_{\rm 1D-2D}$) between FSN and FSR defined by FSN minus FSR. Basemaps are provided by Tianditu (https://map.tianditu.gov.cn/).

of equifinal approaches widen the overall performance gap, as measured by CSI, especially for rainfall events with return periods below 50 years. Regarding BIAS, physical approaches that adopt reconstructed networks but without controls exhibit a consistent underestimation of the total inundated area with BIAS values less than 1. In contrast, other equifinal approaches tend to overestimate the inundated area. Specifically, RDA and NDA can overestimate the total inundated area by more than

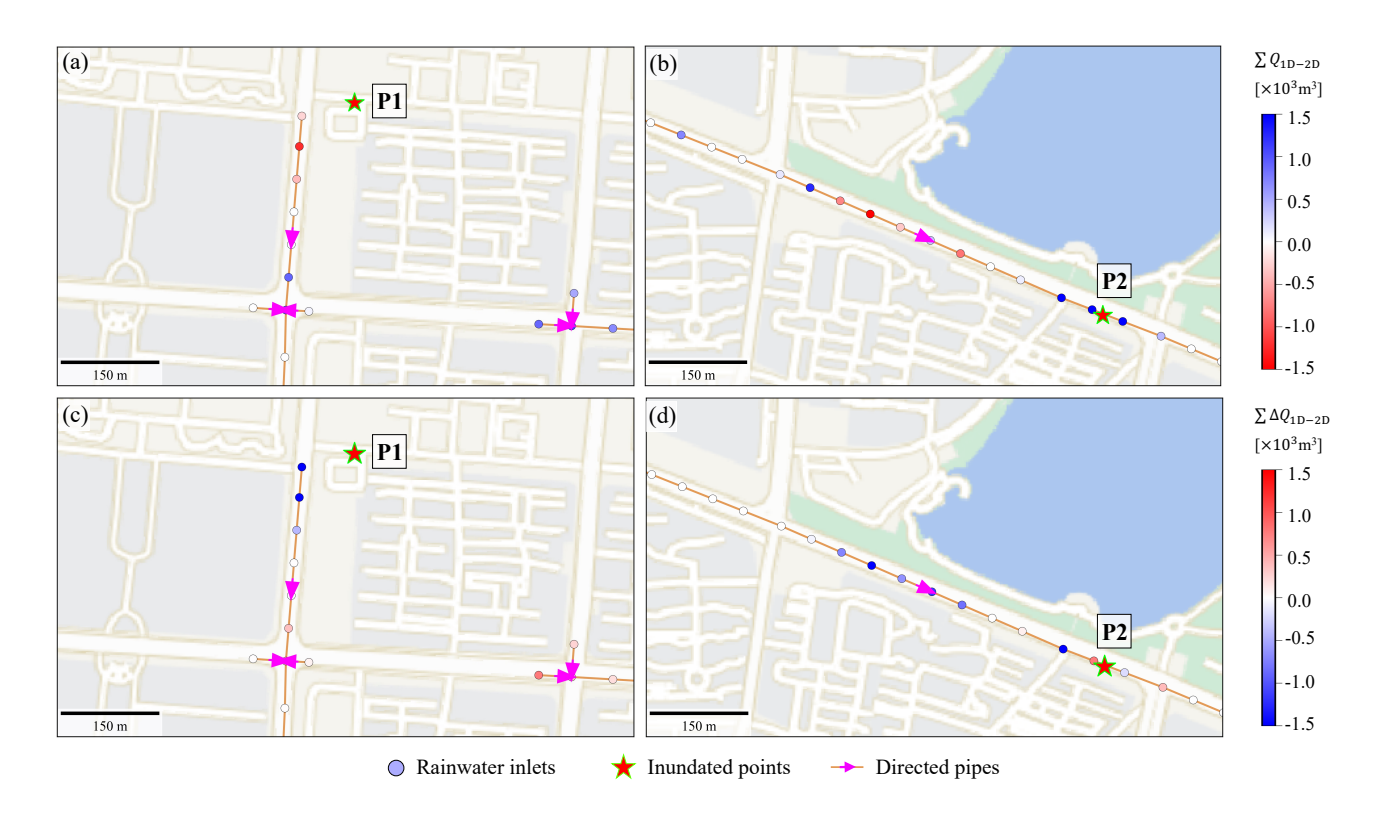


Figure 11. Comparison of accumulated discharges at rainwater inlets during the July 2022 storm. (a)-(b) RSN simulated discharges. (c)-(d) Simulated discharge differences between RSN and FSN defined by RSN minus FSN. Basemaps are provided by Tianditu (https://map.tianditu.gov.cn/).

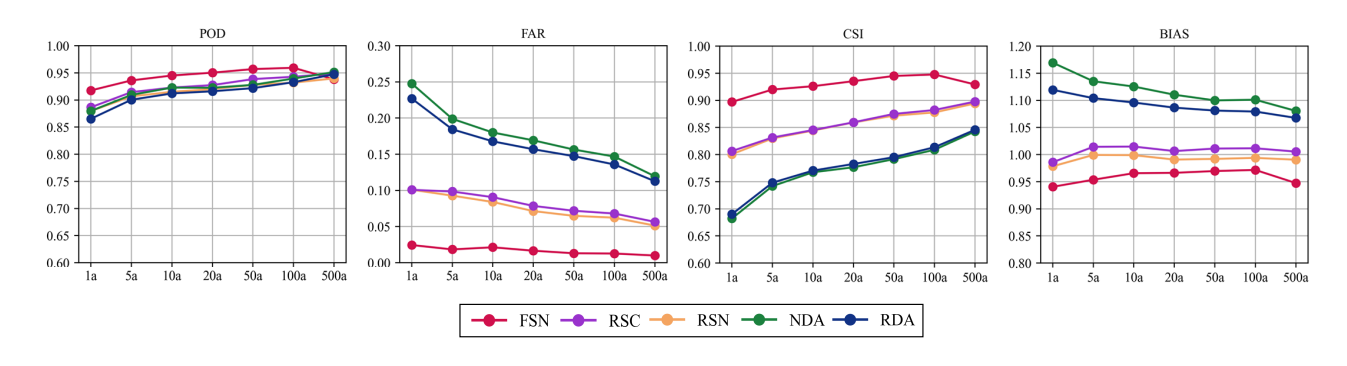


Figure 12. Comparison of simulated inundation area under design rainfall scenarios using different approximation methods.

8% and 10% for rainfall events with return periods less than 100 years, respectively. Thus, a constant equivalent drainage rate is insufficient to achieve an accurate simulation of sewer drainage effects under diverse rainfall conditions, while physical approaches can also yield biased estimation of the inundated area if regulated facilities are not properly configured.

From the perspective of water balance, total inundated areas (or volumes) are closely related to the volume of rainwater drained outside the system. Thus, we further compare the discharge processes at outfalls simulated by different physical approaches (see Fig. S3 in the Supplementary Material). Being the solution reconstructed from the most detailed information, FSR clearly reveals the insufficient drainage capacities at most outfalls such as OF1. When regulated facilities are excluded but sewer layout remains unchanged, FSN demonstrates significantly higher discharges, especially at major outflow points such as OF2 and OF3 with peak flows over 300% higher, thereby leading to an underestimation of total inundated areas (Fig. 12). When the sewer layout is further simplified by the major roads, the simulated outflows decrease by approximately 27% due to reduced inlets that collect rainwater into the sewer system. This attribution can be further supported by the improved alignment of outflow hydrographs between RSN and RSC, which exhibit fewer truncations during peak flows under regulated conditions when compared to FSR and FSN. This indicates an alleviation of drainage deficiency due to reduced rainwater inflow. However, certain outflow points, such as OF3, still yield substantially higher discharges with simplified road networks. Comparison of layouts used in FSN and RSN reveals that a main pipe, measuring 6.8 m \times 2.6 m (near OF1 and OF8, cf. Fig. 13) is found to be removed during simplification, blocking the drainage pathway that divides the corresponding upstream rainwater to the northern outflow points such as OF1 and OF8, eventually magnifying the inflow to OF3. Thus, for real urban environments with complicated sewer layouts due to practical factors such as multistage construction, direct geometric simplification through major roads may remove some critical connectivity inside a graph-like drainage system and thus fail to accurately represent the drainage effects of the sewer network due to topological incompleteness.

4.7 Outlook and limitation

355

360

365

370

375

385

The proposed graph reconstruction-based approach offers an efficient solution for generating physical sewer models using available data on sewer layouts and surface elevation, which can be obtained from local surveys (Xing et al., 2022), engineering drawings (Lyu et al., 2018), or open source software such as SWMManywhere (Dobson et al., 2025). Given the significant influence of network topology and regulation facilities on inundation simulation results (as discussed in Sect. 4.5 and 4.6), in addition to the aforementioned data sources, it is imperative to further implement intelligent surveying systems targeting relevant critical components such as inlets and outfalls. These data can then be integrated with the proposed reconstruction algorithm to achieve more reliable pluvial flood modeling. In particular, outfall identification still remains a difficult task, especially for decentralized sewer networks in relatively flat urban areas, challenging the applicability of existing topography-driven approaches (Dobson et al., 2025) and motivating the need for user-defined configurations according to prior knowledge of the area (Reyes-Silva et al., 2023). In addition, it should be acknowledged that considering inherent quality issues of multi-source geographical datasets, mathematical programming procedures in the proposed approach may occasionally fail because of infeasible configurations such as over-elevated outfalls and dangling pipelines. While introducing data cleaning procedures may help alleviate such issues and streamline the downstreaming reconstruction process, it also necessitates the trade-off between algorithm robustness and accuracy owing to embedded assumptions during quality control, which deserves further investigations. In addition to related cleaning functions implemented in existing packages like SWMManywhere (Dobson et al., 2025), we propose leveraging the built-in functionality of irreducible inconsistent subset (IIS) computation within our optimization-based framework, which can be steadily accessed in solvers such as Gurobi (https://docs.gurobi.com/projects/optimizer). This tool can help identify the specific constraints responsible for infeasibility and thus support the spatial pinpointing of ill-conditioned sewer elements that over-constrain the optimization and may require further correction or elimination. In summary, additional integration with other existing tools will further enhance the practicality of the proposed reconstruction method and facilitate a more realistic representation of drainage effects in urban pluvial flood simulation.

5 Conclusions

390

405

410

415

- In this work, we present a graph reconstruction-based approach for building a physical sewer hydraulic model, leveraging incomplete information and surface elevation model while adhering to design guidelines. In contrast to conventional optimal-design-based approaches, our approach seeks to reconstruct the most possible sewer network with related hydraulic properties, such as gravitional flow direction and nodal invert elevation, constrained by minimal deviation from the initial status based on available information. The resulting mathematical programming problems can be equivalently transformed into corresponding linearized formulations, ensuring their computational efficiency for large-scale applications. We apply the proposed approach to Yinchuan's main city zone, characterized by multiple outfalls consisting of wastewater treatment plants and pump stations, yielding the following key insights:
 - The reconstructed sewer hydraulic module integrated into a 1D/2D coupled hydrologic-hydrodynamic model achieves high accuracy in simulating maximum inundation depths, with an R² of 0.95. A comparison with road-based layout simplifications further demonstrates the robustness of our approach in reconstructing sewer hydraulic properties, as the simplified model maintains a similar distribution of pipe slopes.
 - While equifinal approaches ease parameter calibration by encapsulating complex sewer drainage processes into equivalent drainage rates, the proposed reconstruction approach can reliably achieve superior performance in simulating inundated areas across various rainfall scenarios. This improvement stems from its physically grounded structure in simulating bidirectional interaction between the ground surface and the sewer system, indicating that physical reconstruction is preferable to approximate sewer drainage effects in operational applications.
 - The completeness of available information has non-negligible effects on the simulated hydraulic performance of reconstructed sewer networks. Simplifications involving road-based layouts and regulation facility removal lead to complex deviation patterns in local maximum inundation depths and outflow hydrographs, with both overestimations and underestimations arising from the combined effects of surface microtopography, sewer connectivity modification and regulation facility operation.

In conclusion, we provide an efficient sewer reconstruction approach that improves the simulation and understanding of sewer drainage effects during urban pluvial floods, accounting for varying levels of information completeness. However, uncertainties persist in reconstructed physical models when detailed information on regulated facilities and drainage pathways is

lacking. Thus, future research will focus on integrating advanced techniques, such as data assimilation and intelligent surveying system, with reconstructed physical models to augment the realism of sewer drainage process representation.

Code and data availability. Landuse (https://worldcover2021.esa.int/download). DEM and sewer network information are not publicly available due to the privacy reasons. The snapshot of the source code and compiled application for sewer reconstruction has been archived on Zenodo (https://doi.org/10.5281/zenodo.15522608). And the up-to-date version is available at: https://github.com/LllC-mmd/ASHED_sewerReconstruction.

425

Author contributions. RL conceived the idea and implement the algorithm. JL and JS collected the data. RL, TS, JL, FT, and GN conducted the analysis. RL drafted the manuscript and all authors reviewed and edited the manuscript.

Competing interests. At least one of the (co-)authors is a member of the editorial board of the Hydrology and Earth System Sciences.

Acknowledgements. This work was supported by the Gansu Province Science and Technology Department (22ZD6WA043), Program of Joint 430 Research Institute of Tsinghua University—Ningxia Yinchuan for the Internet of Water and Digital Governance (SKL-IOW-2022TC2010), NERC Independent Research Fellowship (NE/P018637/2).

References

450

- Bakhshipour, A. E., Bakhshizadeh, M., Dittmer, U., Haghighi, A., and Nowak, W.: Hanging Gardens Algorithm to Generate Decentralized Layouts for the Optimization of Urban Drainage Systems, Journal of Water Resources Planning and Management, 145, 04019 034, https://doi.org/10.1061/(ASCE)WR.1943-5452.0001103, 2019.
 - Bakhshipour, A. E., Hespen, J., Haghighi, A., Dittmer, U., and Nowak, W.: Integrating Structural Resilience in the Design of Urban Drainage Networks in Flat Areas Using a Simplified Multi-Objective Optimization Framework, Water, 13, https://doi.org/10.3390/w13030269, 2021.
- Blumensaat, F., Wolfram, M., and Krebs, P.: Sewer model development under minimum data requirements, Environmental Earth Sciences, 65, 1427–1437, https://doi.org/10.1007/s12665-011-1146-1, 2012.
 - Cao, X., Lyu, H., Ni, G., Tian, F., Ma, Y., and Grimmond, C.: Spatial Scale Effect of Surface Routing and Its Parameter Upscaling for Urban Flood Simulation Using a Grid-Based Model, Water Resources Research, 56, e2019WR025468, https://doi.org/10.1029/2019WR025468, e2019WR025468 2019WR025468, 2020.
- Chegini, T. and Li, H.-Y.: An algorithm for deriving the topology of belowground urban stormwater networks, Hydrology and Earth System Sciences, 26, 4279–4300, https://doi.org/10.5194/hess-26-4279-2022, 2022.
 - Chen, Z. and Huang, G.: Numerical simulation study on the effect of underground drainage pipe network in typical urban flood, Journal of Hydrology, 638, 131 481, https://doi.org/10.1016/j.jhydrol.2024.131481, 2024.
 - Dobson, B., Jovanovic, T., Alonso-Álvarez, D., and Chegini, T.: SWMManywhere: A workflow for generation and sensitivity analysis of synthetic urban drainage models, anywhere, Environmental Modelling & Software, 186, 106358, https://doi.org/10.1016/j.envsoft.2025.106358, 2025.
 - Dunton, A. and Gardoni, P.: Generating network representations of small-scale infrastructure using generally available data, Computer-Aided Civil and Infrastructure Engineering, 39, 1143–1158, https://doi.org/10.1111/mice.13137, 2024.
 - Duque, N., Bach, P. M., Scholten, L., Fappiano, F., and Maurer, M.: A Simplified Sanitary Sewer System Generator for Exploratory Modelling at City-Scale, Water Research, 209, 117 903, https://doi.org/10.1016/j.watres.2021.117903, 2022.
- Elimam, A. A., Charalambous, C., and Ghobrial, F. H.: Optimum Design of Large Sewer Networks, Journal of Environmental Engineering, 115, 1171–1190, https://doi.org/10.1061/(ASCE)0733-9372(1989)115:6(1171), 1989.
 - Forrest, J. and Lougee-Heimer, R.: CBC User Guide, chap. Chapter 10, pp. 257–277, INFORMS, https://doi.org/10.1287/educ.1053.0020, 2005.
- Giangrande, S. E., McGraw, R., and Lei, L.: An Application of Linear Programming to Polarimetric Radar Differential Phase Processing,

 Journal of Atmospheric and Oceanic Technology, 30, 1716 1729, https://doi.org/10.1175/JTECH-D-12-00147.1, 2013.
 - Hall, J.: Direct Rainfall Flood Modelling: The Good, the Bad and the Ugly, Australasian Journal of Water Resources, 19, 74–85, https://doi.org/10.7158/13241583.2015.11465458, 2015.
 - Hesarkazzazi, S., Hajibabaei, M., Bakhshipour, A. E., Dittmer, U., Haghighi, A., and Sitzenfrei, R.: Generation of optimal (de)centralized layouts for urban drainage systems: A graph-theory-based combinatorial multi-objective optimization framework, Sustainable Cities and Society, 81, 103 827, https://doi.org/10.1016/j.scs.2022.103827, 2022.
 - Johnson, D. B.: Finding All the Elementary Circuits of a Directed Graph, SIAM Journal on Computing, 4, 77–84, https://doi.org/10.1137/0204007, 1975.

- Järvi, L., Grimmond, C., and Christen, A.: The Surface Urban Energy and Water Balance Scheme (SUEWS): Evaluation in Los Angeles and Vancouver, Journal of Hydrology, 411, 219–237, https://doi.org/10.1016/j.jhydrol.2011.10.001, 2011.
- Kim, S. E., Seo, Y., Hwang, J., Yoon, H., and Lee, J.: Connectivity-informed drainage network generation using deep convolution generative adversarial networks, Scientific Reports, 11, 1519, https://doi.org/10.1038/s41598-020-80300-6, 2021.
 - Krebs, G., Kokkonen, T., Valtanen, M., Setälä, H., and Koivusalo, H.: Spatial resolution considerations for urban hydrological modelling, Journal of Hydrology, 512, 482–497, https://doi.org/10.1016/j.jhydrol.2014.03.013, 2014.
 - Li, D., Hou, J., Xia, J., Tong, Y., Yang, D., Zhang, D., and Gao, X.: An Efficient Method for Approximately Simulating Drainage Capability for Urban Flood, Frontiers in Earth Science, 8, https://doi.org/10.3389/feart.2020.00159, 2020.

- Li, D., Hou, J., Shen, R., Li, B., Tong, Y., and Wang, T.: Approximation method for the sewer drainage effect for urban flood modeling in areas without drainage-pipe data, Frontiers in Environmental Science, 11, https://doi.org/10.3389/fenvs.2023.1134985, 2023.
- Li, G. and Matthew, R. G. S.: New Approach for Optimization of Urban Drainage Systems, Journal of Environmental Engineering, 116, 927–944, https://doi.org/10.1061/(ASCE)0733-9372(1990)116:5(927), 1990.
- 480 Liu, L., Sun, J., and Lin, B.: A large-scale waterlogging investigation in a megacity, Natural Hazards, 114, 1505–1524, https://doi.org/10.1007/s11069-022-05435-3, 2022.
 - Lu, Y., Zhai, G., and Zhou, S.: An integrated Bayesian networks and Geographic information system (BNs-GIS) approach for flood disaster risk assessment: A case study of Yinchuan, China, Ecological Indicators, 166, 112 322, https://doi.org/10.1016/j.ecolind.2024.112322, 2024.
- Luan, G., Hou, J., Wang, T., Zhou, Q., Xu, L., Sun, J., and Wang, C.: Method for analyzing urban waterlogging mechanisms based on a 1D-2D water environment dynamic bidirectional coupling model, Journal of Environmental Management, 360, 121024, https://doi.org/10.1016/i.jenvman.2024.121024, 2024.
 - Lyu, H., Ni, G., Cao, X., Ma, Y., and Tian, F.: Effect of Temporal Resolution of Rainfall on Simulation of Urban Flood Processes, Water, 10, https://doi.org/10.3390/w10070880, 2018.
- 490 Machine Hsie, M.-Y. W. and Huang, C. Y.: Optimal urban sewer layout design using Steiner tree problems, Engineering Optimization, 51, 1980–1996, https://doi.org/10.1080/0305215X.2018.1560436, 2019.
 - McGrath, H., Bourgon, J.-F., Proulx-Bourque, J.-S., Nastev, M., and Abo El Ezz, A.: A comparison of simplified conceptual models for rapid web-based flood inundation mapping, Natural Hazards, 93, 905–920, https://doi.org/10.1007/s11069-018-3331-y, 2018.
- Mitchell, S., OSullivan, M., and Dunning, I.: Pulp: a linear programming toolkit for python, The University of Auckland, Auckland, New Zealand, 65, 25, 2011.
 - MOHURD: Standard for Design of Outdoor Wastewater Engineering, GB 50014-2021, Ministry of Housing and Urban-Rural Development of the People's Republic of China, Beijing, China, in Chinese, 2021.
 - Montalvo, C., Reyes-Silva, J., Sañudo, E., Cea, L., and Puertas, J.: Urban pluvial flood modelling in the absence of sewer drainage network data: A physics-based approach, Journal of Hydrology, 634, 131 043, https://doi.org/10.1016/j.jhydrol.2024.131043, 2024.
- Ni, G.-H., Liu, Z.-Y., Lei, Z.-D., Yang, D.-W., and Wang, L.: Continuous Simulation of Water and Soil Erosion in a Small Watershed of the Loess Plateau with a Distributed Model, Journal of Hydrologic Engineering, 13, 392–399, https://doi.org/10.1061/(ASCE)1084-0699(2008)13:5(392), 2008.
- Perrini, P., Cea, L., Chiaravalloti, F., Gabriele, S., Manfreda, S., Fiorentino, M., Gioia, A., and Iacobellis, V.: A Runoff-On-Grid Approach to Embed Hydrological Processes in Shallow Water Models, Water Resources Research, 60, e2023WR036421, https://doi.org/10.1029/2023WR036421, e2023WR036421 2023WR036421, 2024.

- Reyes-Silva, J. D., Novoa, D., Helm, B., and Krebs, P.: An Evaluation Framework for Urban Pluvial Flooding Based on Open-Access Data, Water, 15, https://doi.org/10.3390/w15010046, 2023.
- Rosenzweig, B. R., McPhillips, L., Chang, H., Cheng, C., Welty, C., Matsler, M., Iwaniec, D., and Davidson, C. I.: Pluvial flood risk and opportunities for resilience, WIREs Water, 5, e1302, https://doi.org/10.1002/wat2.1302, 2018.
- 510 Rossman, L. A.: Storm Water Management Model User's Manual Version 5.1, U.S. Environmental Protection Agency, 2015.

- Rossman, L. A. and Huber, W.: Storm Water Management Model Reference Manual Volume II Hydraulics, US Environmental Protection Agency: Washington, DC, USA, 2, 190, 2017.
- Safavi, H. and Geranmehr, M. A.: Optimization of sewer networks using the mixed-integer linear programming, Urban Water Journal, 14, 452–459, https://doi.org/10.1080/1573062X.2016.1176222, 2017.
- 515 Schmitt, T. G. and Scheid, C.: Evaluation and communication of pluvial flood risks in urban areas, WIREs Water, 7, e1401, https://doi.org/10.1002/wat2.1401, 2020.
 - Schubert, J. E. and Sanders, B. F.: Building treatments for urban flood inundation models and implications for predictive skill and modeling efficiency, Advances in Water Resources, 41, 49–64, https://doi.org/10.1016/j.advwatres.2012.02.012, 2012.
 - Shi, X., Liu, Z., Carlos, V., and Jia, H.: The role of graph-based methods in urban drainage networks (UDNs): review and directions for future, Urban Water Journal, 20, 1095–1109, https://doi.org/10.1080/1573062X.2023.2252807, 2023.
 - Sitzenfrei, R., Wang, Q., Kapelan, Z., and Savić, D.: Using Complex Network Analysis for Optimization of Water Distribution Networks, Water Resources Research, 56, e2020WR027929, https://doi.org/10.1029/2020WR027929, e2020WR027929 2020WR027929, 2020.
 - Song, L., Zhou, J., Guo, J., Zou, Q., and Liu, Y.: A robust well-balanced finite volume model for shallow water flows with wetting and drying over irregular terrain, Advances in Water Resources, 34, 915–932, https://doi.org/10.1016/j.advwatres.2011.04.017, 2011.
- 525 Swamee, P. K. and Sharma, A. K.: Optimal design of a sewer line using Linear Programming, Applied Mathematical Modelling, 37, 4430–4439, https://doi.org/10.1016/j.apm.2012.09.041, 2013.
 - Tran, V. N., Ivanov, V. Y., Huang, W., Murphy, K., Daneshvar, F., Bednar, J. H., Alexander, G. A., Kim, J., and Wright, D. B.: Connectivity in urbanscapes can cause unintended flood impacts from stormwater systems, Nature Cities, 1, 654–664, https://doi.org/10.1038/s44284-024-00116-7, 2024.
- Wagner, H. M.: Linear Programming Techniques for Regression Analysis, Journal of the American Statistical Association, 54, 206–212, https://doi.org/10.1080/01621459.1959.10501506, 1959.
 - Wang, J., Liu, J., Mei, C., Wang, H., and Lu, J.: A multi-objective optimization model for synergistic effect analysis of integrated green-gray-blue drainage system in urban inundation control, Journal of Hydrology, 609, 127725, https://doi.org/10.1016/j.jhydrol.2022.127725, 2022.
- Wang, Q., Savić, D. A., and Kapelan, Z.: GALAXY: A new hybrid MOEA for the optimal design of Water Distribution Systems, Water Resources Research, 53, 1997–2015, https://doi.org/10.1002/2016WR019854, 2017.
 - Wang, S. and Wang, H.: Extending the Rational Method for assessing and developing sustainable urban drainage systems, Water Research, 144, 112–125, https://doi.org/10.1016/j.watres.2018.07.022, 2018.
- Weng, Q.: Remote sensing of impervious surfaces in the urban areas: Requirements, methods, and trends, Remote Sensing of Environment, 117, 34–49, https://doi.org/10.1016/j.rse.2011.02.030, remote Sensing of Urban Environments, 2012.
 - Xing, Y., Liang, Q., Wang, G., Ming, X., and Xia, X.: City-scale hydrodynamic modelling of urban flash floods: the issues of scale and resolution, Natural Hazards, 96, 473–496, https://doi.org/10.1007/s11069-018-3553-z, 2019.

- Xing, Y., Shao, D., Yang, Y., Ma, X., and Zhang, S.: Influence and interactions of input factors in urban flood inundation modeling: An examination with variance-based global sensitivity analysis, Journal of Hydrology, 600, 126 524, https://doi.org/10.1016/j.jhydrol.2021.126524, 2021.
 - Xing, Y., Shao, D., Liang, Q., Chen, H., Ma, X., and Ullah, I.: Investigation of the drainage loss effects with a street view based drainage calculation method in hydrodynamic modelling of pluvial floods in urbanized area, Journal of Hydrology, 605, 127 365, https://doi.org/10.1016/j.jhydrol.2021.127365, 2022.
- Yu, X., Wu, Y., Meng, F., Zhou, X., Liu, S., Huang, Y., and Wu, X.: A review of graph and complex network theory in water distribution networks: Mathematical foundation, application and prospects, Water Research, 253, 121 238, https://doi.org/10.1016/j.watres.2024.121238, 2024.
 - Zanaga, D., Van De Kerchove, R., Daems, D., De Keersmaecker, W., Brockmann, C., Kirches, G., Wevers, J., Cartus, O., Santoro, M., Fritz, S., et al.: ESA WorldCover 10 m 2021 v200, https://doi.org/10.5281/zenodo.7254221, 2022.

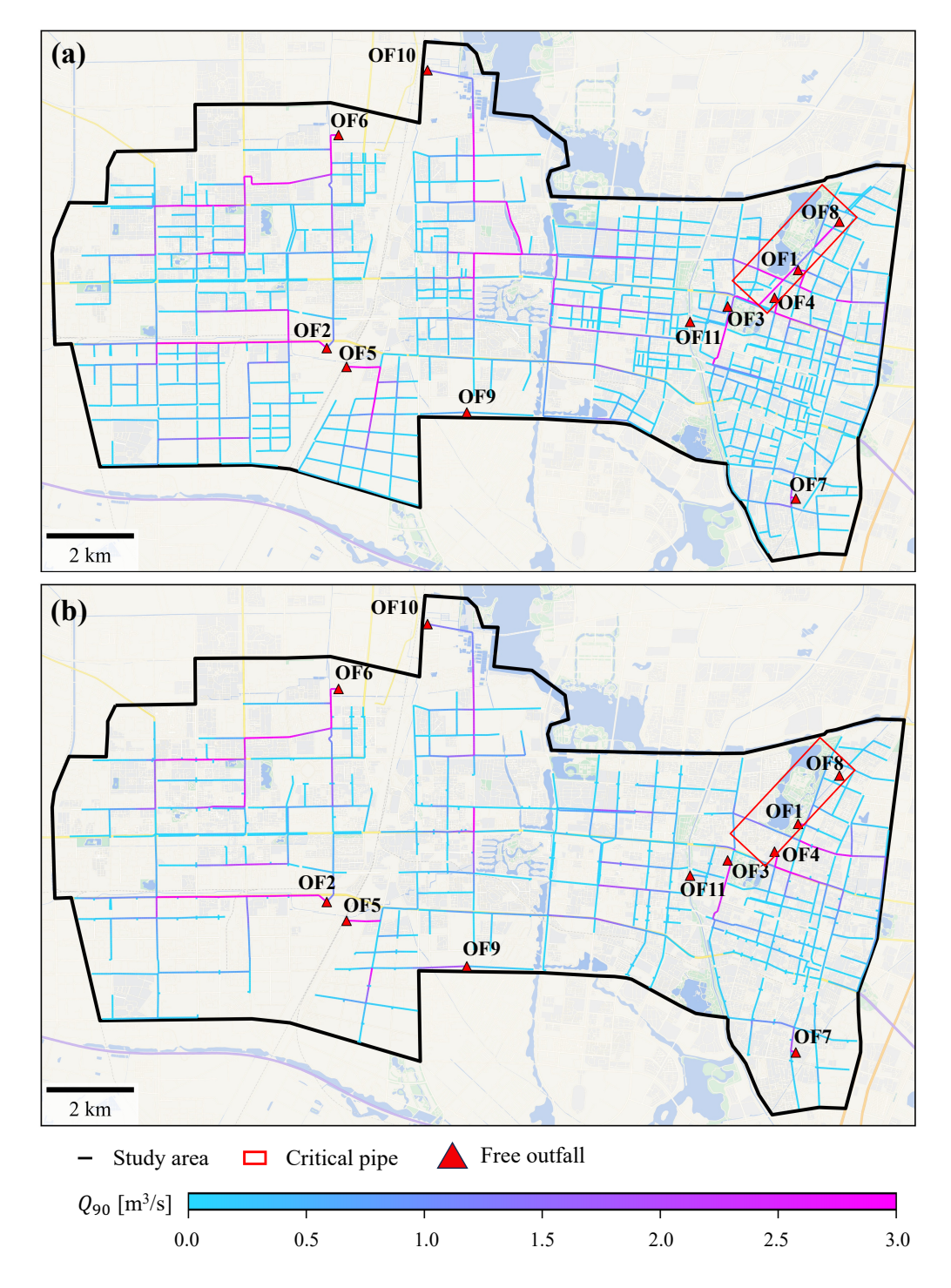


Figure 13. Comparison of simulated flows at 90 percentiles (Q_{90}) of pipes under design rainfall scenarios using physical approaches with-/without network simplification. (a) FSN approach. (b) RSN approach. Basemaps are provided by Tianditu (https: //map.tianditu.gov.cn/).